# AN OPTIMUM SCREW PROPELLER WITH ENDPLATES

by

J.A. Sparenberg and J. de Vries

# AN OPTIMUM SCREW PROPELLER WITH ENDPLATES


## Summary

In this paper is discussed the design of an optimum screw propeller model with endplates at the tips of the blades, based on a linear optimization theory. Results of experiments are given.


## 1. Introduction

We discuss the design of a screw propeller with endplates at the tips of its blades. The method of design takes into account the interaction of blades and endplates. The circulation around these lifting surfaces is determined by the linear optimization theory as described in [1].

A draw back of endplates is that they move with a large velocity through the fluid and hence give rise to relatively large viscous losses. Besides this the tips of the blades have to be broad which also increases the viscous losses. The gain in efficiency is caused by spreading more evenly the tip vortices by which the loss of kinetic energy E per unit of time becomes smaller. We can write $E = \text{const.}\ T^2/q$, where T is the thrust and q is the quality number of the propeller. The quality number of the propeller we consider, varies from $q = \pm 0.65$ when endplates are absent, to $q = \pm 0.84$ when the "ratio of covering" (see section 5) of the endplates is equal to 1. The formula shows that the endplates will become more effective in case of a heavily loaded propeller, because then T is large and E can be reduced by constructing a propeller with a large quality number q. On the other hand larger values of q demand endplates with a larger span, hence more viscous resistance. So here also an optimum has to be sought.

The theory we apply suffers from the disadvantage that it is a linearized one and seemingly not adequate for heavily loaded propellers. Nevertheless, for lack of a non-linear optimization theory, we have used the linear one. Experiments show that the model designed by means of this theory can at least compete with a corresponding three bladed propeller from the B-screw series, which has the same blade area ratio, advance coefficient and thrust coefficient as our model propeller in its design situation. For values of the velocity of advance which are below the design value, while the rotational velocity of the propeller is kept the same, the thrust increases and then it is seen that the efficiency of the propeller with endplates becomes significantly better than the efficiency of the corresponding B-screw series propeller.

An argument which is sometimes heard against propellers with endplates is that such a propeller does not behave well behind a ship. This did not happen with our model propeller when it was tested in the wake of a ship model.

## 2. Design criteria for the propeller model

We first list the design criteria for the screw propeller model.

| | | | |
|---|---|---|---|
| Diameter of propeller | : | $D = 2R = 0.2$ m, | (2.1) |
| Diameter of hub | : | $D_h = 2R_h = 0.04$ m, | (2.2) |
| Number of blades | : | $Z = 3$, | (2.3) |
| Revolutions per second | : | $N = 18.75$/sec, | (2.4) |
| Thrust | : | $T = 200$ Newton, | (2.5) |
| Velocity of advance | : | $U = 3$ m/sec, | (2.6) |
| Blade area ratio | : | $A_e/\pi R^2 = 0.65$, | (2.7) |
| Rake angle | : | $0^o$, | (2.8) |

where $A_e$ is the expanded blade area.

## 3. The blade

We consider a cylindrical system (x,r,θ) (figure 3.1).
With respect to this reference system we have an incoming flow parallel

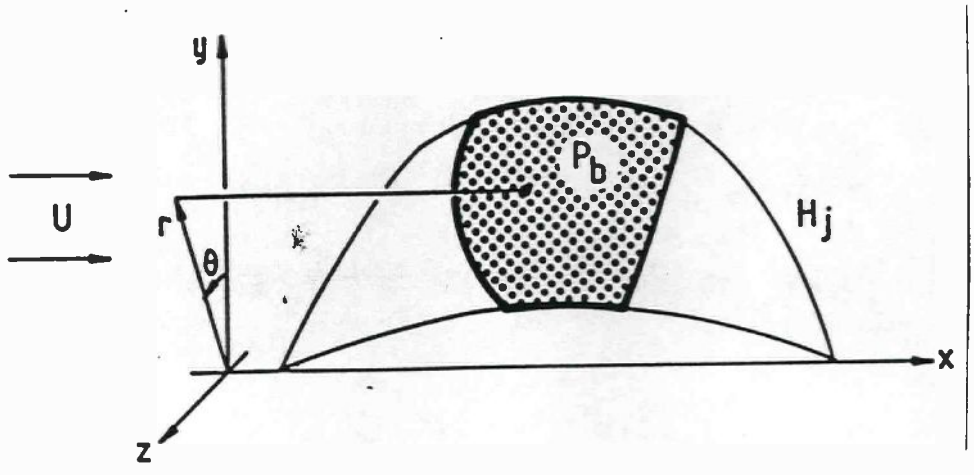


Fig. 3.1. Helicoidal surface $H_j$ with planform $P_b$ of blade.

to the x-axis with the velocity U = 3 m/sec and three rotating helicoidal surfaces $H_j$

$$H_j\ (x,r,\theta,t) = \theta - \omega t + ax = \alpha_j,\ \alpha_j = \frac{2(j-1)\pi}{3},\ j = 1,2,3, \qquad (3.1)$$

where ω = 117.81 rad/sec and (2.6) a = ω/U = 39.27/m. These surfaces do not disturb the parallel flow.

By the planform $P_b$ of a blade we understand its projection on the neighbouring helicoidal surface $H_j$, a profile of a blade at radius r is the intersection of the blade with a cylinder of radius r around the x-axis. An expanded blade is drawn in figure 3.2, its shape upto r/R = 0.8 is the same as that of the B-screw series but has a finite chordlength (7.5 cm) at the tip, in order to be able to apply the endplate. The thickness distribution of the profiles is the same as is used for the B-screw series.

The maximum thickness $h_{mb}$ of the profiles is chosen to be a linear function of r/R

$$h_{mb}(\frac{r}{R}) = (0.85 - 0.25\,\frac{r}{R})\ \text{cm}. \qquad (3.2)$$

Hence at the root of the blade (r/R = 0.2) the maximum thickness is 0.8 cm and at the tip (r/R = 1) it is 0.6 cm.

The camber of the profiles follows by lifting surface theory from the calculated optimum circulation distributions in spanwise direction along blades and endplates, from the chosen load distribution in chordwise direction, from the thickness distributions and from the geometry of blades and endplates.

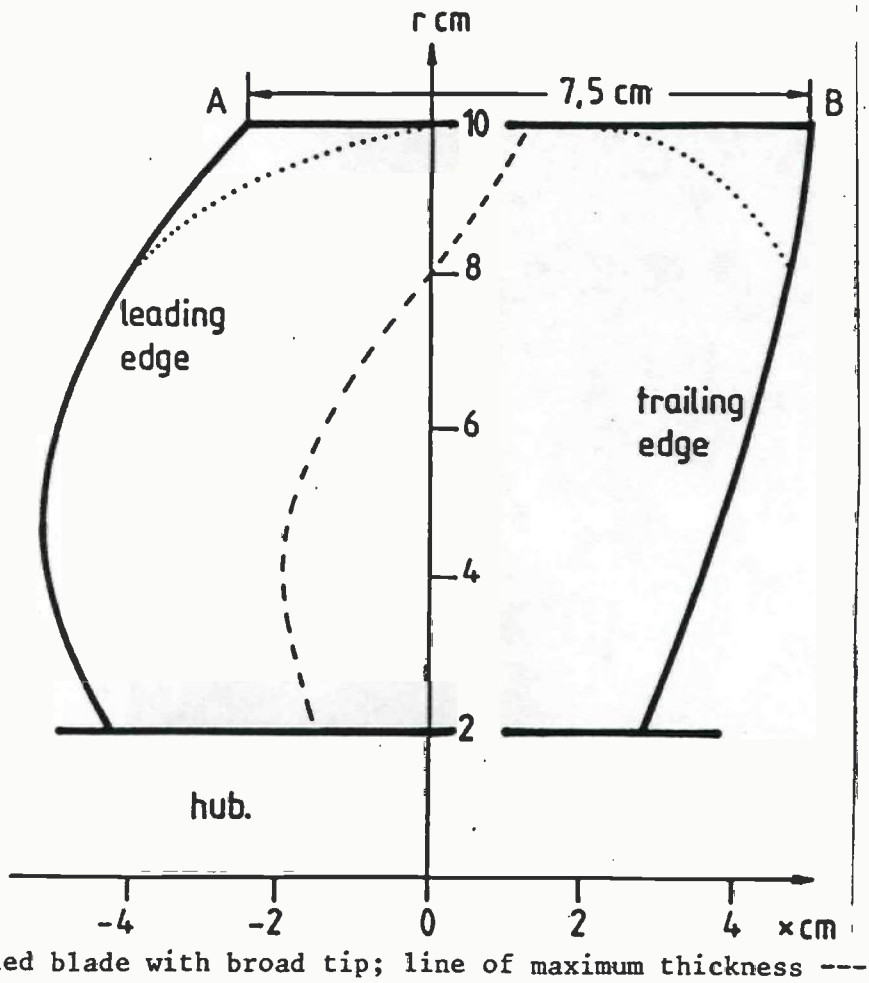


Fig. 3.2. Expanded blade with broad tip; line of maximum thickness ---; B-screw series, chord wise multiplied by 0.95..... .

## 4. The endplate.

The planform $P_e$ of an endplate is the projection of the endplate on the cylinder with radius r = R = 0.1 m which passes through the tips of the propeller blades and of which the axis coincides with the x-axis. A profile of the endplate is the intersection of the endplate with a helicoidal surface $\theta + ax = \theta^*$ for some value of $\theta^*$, where we take t = 0 in (3.1). By the chordlength of a profile at a certain value of $\theta^*$ we understand the length of the helicoidal line, which is the intersection of the helicoidal surface $\theta + ax = \theta^*$ and the cylinder r = R = 0.1, in between the leading edge and the trailing edge of the endplate. In contradistinction with the helicoidal planform of the blade, the cylindrical planform of the endplate can be developed. An endplate has two sides, the inner side which is directed towards the axis of the propeller, the other side we call the outer side.

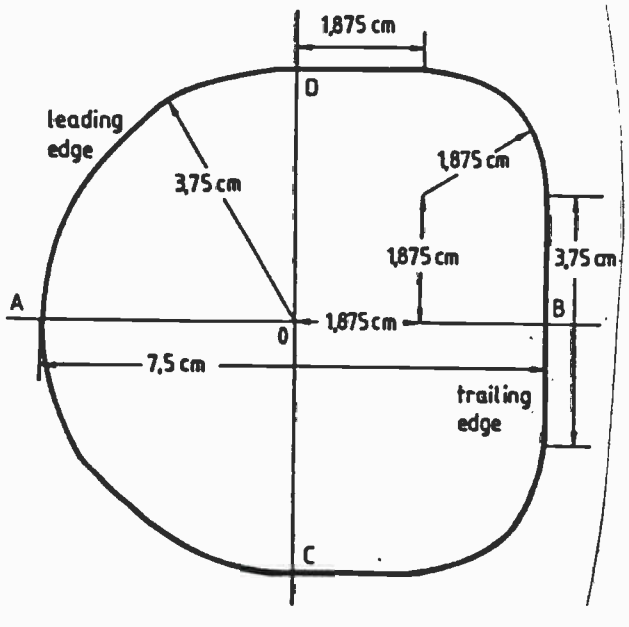


Fig. 4.1. Developed basic planform of endplate.

The chosen shape of the developed basic planform of an endplate is drawn in figure 4.1. The length of the mid-chord (AB) is 7.5 cm is

equal to the chord length of the tip profile of a blade. This mid-chord is in the three dimensional space, part of one of the helicoidal lines (3.2) with r = 0.1 m. The developed basic endplate possesses a leading edge which is a semi-circle of radius 3.75 cm. The trailing edge consists of two quarter circles of radius 1.875 cm and tangent to them a straight line segment of length 3.75 cm. The straight tips have a chordlength of 1.875 cm. The total span is 7.5 cm.

In the realization of the screw propeller with endplates we will consider endplates of which, in view of their viscous resistance (section 6), the span is smaller than 7.5 cm. These planforms will have a developed shape which follows from the developed basis planform of figure 4.1, by multiplying the dimensions of figure 4.1, perpendicular to (AB) by some positive number $\mu < 1$.

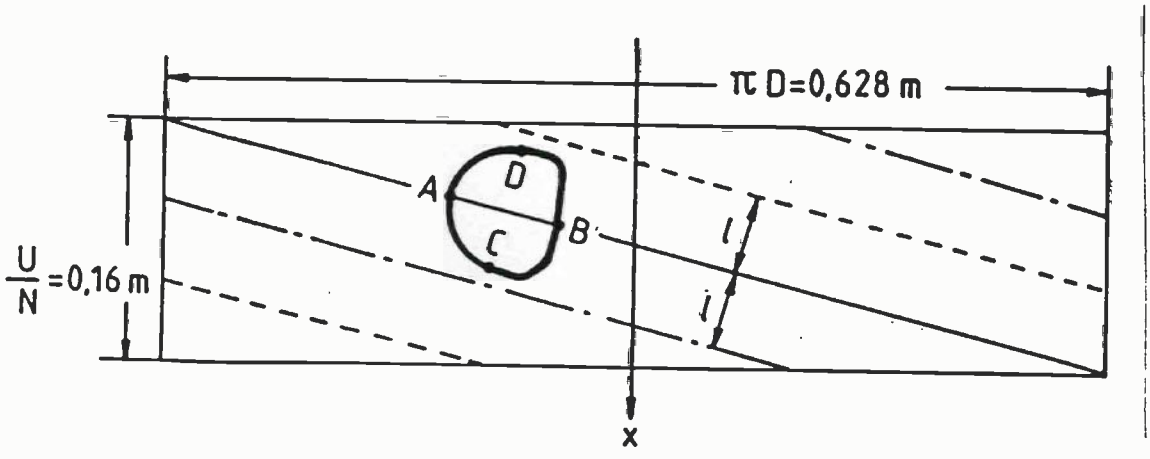


Fig. 4.2. Developed cylinder r = 0.1 m, with basic planform of endplate; path of blade tip (AB) ———, paths of the two other tips -.-.-.-.- and ----.

We first determine (figure 4.2) the distance $\ell$ between the path of blade tip (AB) and the paths of the two other blade tips. We find

$$\ell = \pi D \frac{U}{3N} \{(\pi D)^2 + (\frac{U}{N})^2\}^{-\frac{1}{2}} = 5.17 \text{ cm.} \qquad (4.1)$$

Hence when we take $\mu = 5.17/7.5 = 0.689$ and multiply the transverse dimensions of the developed basic planform by this value then, in the linearized theory, the tip vortices of one endplate will coincide behind the propeller with the adjacent tip vortices of the other two. In other words, the helicoidal strips behind the spans of the endplates just "cover" together the whole cylinder of radius $r = 0.1$ m. When we take $\mu < 0.689$, then only part of this cylinder is covered. The total span of the endplate is denoted by $2\Sigma = 7.5\ \mu$ cm.

We now consider the thickness distribution $w_p$ of the endplate. We introduce the length parameter $\sigma$ in spanwise direction along the endplate, perpendicular to the helicoidal lines on the cylinder $r = 0.1$ m, with $\sigma = 0$ at the midchord (AB), $0 < \sigma \leq \Sigma$ at that half of the endplate which is at the low pressure side of the blade and $-\Sigma \leq \sigma < 0$ at the other half of the endplate.

Independently of the span of the endplate, hence independently of the value we give to the factor $\mu$, the maximum thickness $h_{mp}$ of a profile of the endplate at the midchord (AB) is 0.25 cm and the maximum thickness of the profile at the tip of the endplate is 0.1 cm. This maximum thickness changes in between midchord and tip linearly with $\sigma$, hence

$$h_{mp}\left(\frac{\sigma}{\Sigma}\right) = \left(0.25 \mp 0.15\ \frac{\sigma}{\Sigma}\right) \text{ cm} \qquad , \quad \sigma \gtrless 0 \ . \tag{4.2}$$

Along each profile of the endplate we choose a parameter $s^*$, with $s^* = 0$ at the leading edge, $s^* = 1$ at the trailing edge and which varies linearly with length. The thickness distribution $h_p(s^*)$ of all profiles of the endplate is the same namely the "Naca 66-006, basic thickness form",

Table 4.1. Thickness distribution $h_p(s^*)$, Naca 66-006.

| $s^*$ | 0.0000 | 0.0050 | 0.0075 | 0.0125 | 0.0250 | 0.0500 | 0.0750 | 0.1000 | 0.1500 | 0.2000 | 0.2500 | 0.3000 | 0.3500 |
|---|---|---|---|---|---|---|---|---|---|---|---|---|---|
| $h_p$ | 0.000. | 0.461. | 0.554. | 0.693 | 0.918 | 1.257 | 1.524 | 1.752 | 2.119 | 2.401 | 2.618 | 2.782 | 2.899 |
| $s^*$ | 0.4000 | 0.4500 | 0.5000 | 0.5500 | 0.6000 | 0.6500 | 0.7000 | 0.7500 | 0.8000 | 0.8500 | 0.9000 | 0.9500 | 1.0000 |
| $h_p$ | 2.971 | 3.000 | 2.985 | 2.925 | 2.815 | 2.611 | 2.316 | 1.953 | 1.543 | 1.107 | 0.665 | 0.262 | 0.000 |

which is given in table 4.1, where the maximum thickness is 3. Hence we find for the thickness distribution $w_p$ of the endplate

$$w_p(\frac{\sigma}{\Sigma}, s^*) = \frac{1}{3} h_p(s^*) h_{mp}(\frac{\sigma}{\Sigma}) \text{ cm.} \tag{4.3}$$

Herewith, for some choice of the factor $\mu$, the planform of the endplate and its thickness distribution is determined.

## 5. Optimum circulation distribution and bound vorticity.

We start with a discussion of the optimum circulation distributions around the blades and around the endplates. The linear optimization theory for this type of propeller is discussed in [1]. We shortly recapitulate the results.

Consider the three helicoidal strips, which are passed through by the planforms of the three blades, and which are described by the equations

$$\theta + ax + \frac{(n-1)}{3} 2\pi = 0; \; -\infty < x < \infty; \; 0.02 \text{ m} \leq r \leq 0.1 \text{ m}; \; n = 1,2,3. \tag{5.1}$$

Next consider the three strips at the cylinder $r = 0.1$ m, passed through by the planforms of the endplates,

$$-ax - \frac{(n-1)}{3} 2\pi - \tilde{\theta} \leq \theta \leq -ax - \frac{(n-1)}{3} 2\pi + \tilde{\theta}; \; -\infty < x < \infty;$$

$$r = 0.1 \text{ m}; \; n = 1,2,3, \tag{5.2}$$

where $\tilde{\theta}$ is a measure for the half span $\Sigma$ of the endplate. It follows from figure 4.2 that $\tilde{\theta} = 1.45 \mu\pi/3$ rad $= 1.52 \mu$ rad. Finally we assume the hub to be a two sided infinite cylinder

$$r = 0.02 \text{ m}; \quad -\infty < x < \infty. \tag{5.3}$$

We translate with a velocity $\lambda$ the surfaces (5.1), (5.2) and (5.3) in the direction of the x-axis, as rigid impermeable surfaces in an unbounded inviscid and incompressible fluid. Then we calculate by solving a Neumann problem, the vorticity on these surfaces. This problem has to be solved under the condition that the cirulation along a contour which encircles the whole configuration, is zero. By this the Neumann problem has a unique solution and yields vorticity which is proportional to $\lambda$. Giving an appropriate value to $\lambda$, as will be discussed directly, the vorticity on the surfaces (5.1) and (5.2) is the free vorticity shed by the optimum propeller of which the specifications are given in section 2.

The calculation of this vorticity has been carried out by the vortex lattice method. On the surfaces (5.1), (5.2) and (5.3) are situated a finite number of suitably placed concentrated helicoidal vortices. In between these vortices and on the surfaces are placed the collocation points at which the boundary conditions for the impermeability of the surfaces is satisfied. By the "helicoidal symmetry" this has to be done at one cross-section of the surfaces (5.1), (5.2) and (5.3) by a plane perpendicular to the x-axis (figure 5.1). It is shown in [1] that only within or where it occurs at the boundary of the denoted angle of $60^{\circ}$, the vorticity has to be considered as unknown. The vorticity at the

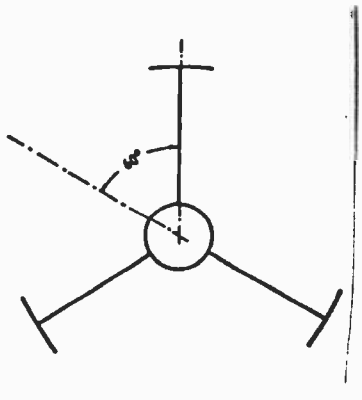

Fig. 5.1. Cross section of the surfaces (5.1), (5.2) and (5.3).

remaining surfaces or at parts of them follow by symmetry or anti-symmetry.

By calculating the momentum of the fluid in the x-diretion caused by the mentioned vorticity, the unknown factor $\lambda$ can be determined so that theoretically the desired thrust of 200 Newton will be delivered. Integrating in an appropriate way the now known shed free vorticity, the circulation $\Gamma_b(r)$ around the blades and the circulation $\Gamma_p(\sigma)$ around the endplates is obtained.

We now introduce the ratio of covering k of the cylinder of radius r = R = 0.1 m through the tips of the blades, by the strips given in (5.2)

$$k = \frac{3\tilde{\theta}}{\pi} \quad , \qquad 0 \leq k \leq 1. \tag{5.4}$$

From figure 4.2 we find the values of $\mu$, $\Sigma$ and k which correspond to each other, they are given in table 5.1.

Table 5.1, Corresponding values $\mu$, $\Sigma$ and k.

| | | | | | |
|---|---|---|---|---|---|
| $\mu$ | 0.689 | 0.517 | 0.345 | 0.172 | |
| $\Sigma$ | 2.58 | 1.94 | 1.30 | 0.65 | cm |
| k | 1.00 | 0.75 | 0.50 | 0.25 | |

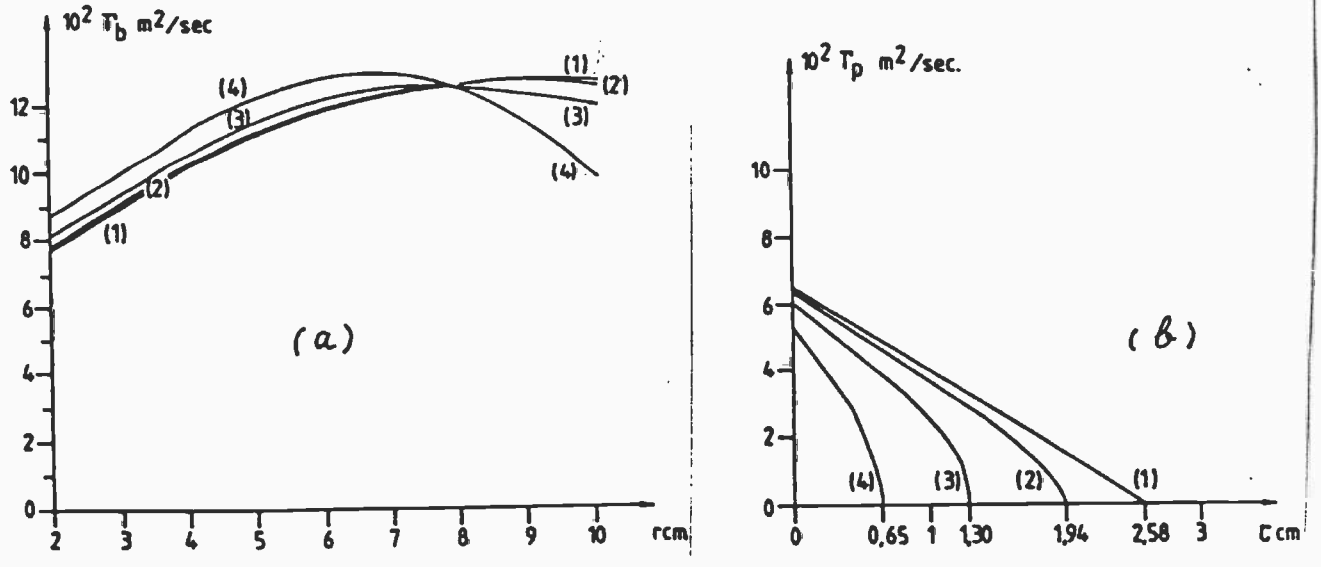


Fig. 5.2. Optimum circulation distributions; (a), $\Gamma_b$ along blades; (b), $\Gamma_p$ along endplates, (1) k = 1.00; (2) k = 0.75; (3) k = 0.50; (4) k = 0.25.

For k = 1, 0.75, 0.50, 0.25, we have calculated the optimum circulation distributions $\Gamma_b(r)$ for the blades and $\Gamma_p(\sigma) = -\Gamma_p(-\sigma)$ for the endplates. These are drawn in figure (5.2) and their numerical values are given in tables 5.2 and 5.3.

Table 5.2. $10^2\Gamma_b(r)$ $m^2$/sec, along span of blade.

| k | 2.25 | 2.75 | 3.25 | 3.75 | 4.25 | 4.75 | 5.25 | 5.75 | 6.25 | 6.75 | 7.25 | 7.75 | 8.25 | 8.75 | 9.25 | 9.75 | r cm |
|---|---|---|---|---|---|---|---|---|---|---|---|---|---|---|---|---|---|
| 1.00 | 8.089 | 8.632 | 9.260 | 9.862 | 10.40 | 10.88 | 11.28 | 11.62 | 11.91 | 12.16 | 12.35 | 12.51 | 12.63 | 12.72 | 12.76 | 12.70 | |
| 0.75 | 8.177 | 8.724 | 9.357 | 9.962 | 10.50 | 10.97 | 11.37 | 11.71 | 11.98 | 12.20 | 12.37 | 12.50 | 12.58 | 12.62 | 12.63 | 12.58 | |
| 0.50 | 8.484 | 9.049 | 9.699 | 10.32 | 10.86 | 11.33 | 11.71 | 12.02 | 12.25 | 12.40 | 12.49 | 12.49 | 12.43 | 12.29 | 12.12 | 12.03 | |
| 0.25 | 9.098 | 9.699 | 10.39 | 11.03 | 11.59 | 12.05 | 12.42 | 12.68 | 12.84 | 12.89 | 12.83 | 12.62 | 12.26 | 11.72 | 11.04 | 10.39 | |

Table 5.3. $10^2\Gamma_p(\sigma/\Sigma)$ $m^2$/sec, along span of endplate.

| k | 0.05 | 0.15 | 0.25 | 0.35 | 0.45 | 0.55 | 0.65 | 0.75 | 0.85 | 0.9375 | $\sigma/\Sigma$ |
|---|---|---|---|---|---|---|---|---|---|---|---|
| 1.00 | 6.052 | 5.387 | 4.757 | 4.123 | 3.490 | 2.857 | 2.227 | 1.600 | 0.982 | 0.434 | |
| 0.75 | 6.013 | 5.517 | 5.009 | 4.494 | 3.972 | 3.442 | 2.898 | 2.330 | 1.719 | 1.044 | |
| 0.50 | 5.770 | 5.364 | 4.947 | 4.518 | 4.088 | 3.610 | 3.118 | 2.582 | 1.970 | 1.241 | |
| 0.25 | 4.985 | 4.679 | 4.361 | 4.028 | 3.675 | 3.297 | 2.885 | 2.422 | 1.874 | 1.196 | |

We now consider a flat actuator disk perpendicular to the x-axis consisting of a circular ring with outer radius r = R = 0.1 m and with inner radius r = $R_h$ = 0.02 m, hence its area $A_a$ = 0.0302 $m^2$. The disk has the same velocity of advance U = 3 m/sec as our propeller model and yields the same total thrust T = 200 Newton, which is uniformly distributed over the area of the disk. We denote the energy loss per sec of our screw propeller by $E_s$ and the energy loss per sec of the disk by $E_a$. Then we define the quality number q of our screw propeller

model as

$$q = E_a/E_s. \tag{5.5}$$

From [1] it follows first, that q is independent of the thrust T, second, that $q \leq 1$ and third, that $E_a$ is equal to

$$E_a = \frac{T^2}{2\rho U A_a} = 221 \text{ Newton m/sec.} \tag{5.6}$$

Then the potential theoretical efficiency $\tilde{\eta}$ of the screw propeller can be written as

$$\tilde{\eta} = \frac{TU}{TU + E_s} = (1 + \frac{E_a}{qTU})^{-1} = (1 + \frac{T}{2\rho q U^2 A_a})^{-1} = (1 + \frac{0.368}{q})^{-1}. \tag{5.7}$$

We note that the efficiency is always the efficiency in the design situation, with the exception of section 8 where also or even mostly experimental results for off-design conditions are given.

From the optimum circulation distributions as given in tables 5.2 and 5.3 it is possible to calculate the lost kinetic energy $E_s$ and hence the quality number q as a function of for instance the ratio of covering k. The results are given in table 5.4 where we added the value of q for k = 0, hence when no endplates are applied. Also in this table we give

Table 5.4. Quality number q and efficiency $\tilde{\eta}$.

| k | 1.00 | 0.75 | 0.50 | 0.25 | 0.00 | |
|---|---|---|---|---|---|---|
| q | 0.838 | 0.827 | 0.793 | 0.734 | 0.648 | |
| $\tilde{\eta}$ | 0.695 | 0.692 | 0.683 | 0.666 | 0.638 | T = 200 Newton |

the efficiency $\tilde{\eta}$ (inviscid fluid) of the screw propeller. From this table it follows that q and for the fixed value of T also $\tilde{\eta}$ increase with k. However it follows from (5.7) that the increase of the efficiency $\tilde{\eta}$ becomes more important for larger values of the demanded thrust T. Hence endplates become more important for heavily loaded propellers, unfortunately then

our linearized theory becomes less reliable.

Finally we discuss how the optimum circulation distributions $\Gamma_b$ and $\Gamma_p$ as given in tables 5.2 and 5.3, are distributed as vorticity $\tilde{\gamma}_b$ and $\tilde{\gamma}_p$ respectively, per unit of length in chordwise direction, where $\tilde{\gamma}_b$ or $\tilde{\gamma}_p$ is the component of the local vorticity at blade or endplate which is perpendicular to the direction of the chord. This has been done both for the profiles of the blades and for the profiles of the endplates in the same way, as is drawn in figure 5.3. If the chordlength is c, then $\tilde{\gamma}(\tilde{\gamma}_b$ or $\tilde{\gamma}_p)$ increases linearly from 0 at the leading edge to its maximum value $\tilde{\gamma}_m$ at the point 0.1 c. The vorticity then remains constant upto

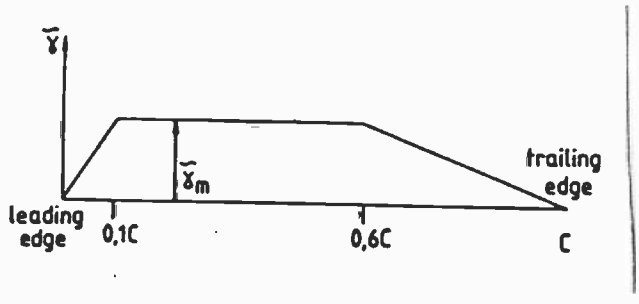


Fig. 5.3. Chordwise distribution of vorticity.

0.6 c and then decreases linearly to zero at the trailing edge. The value $\tilde{\gamma}_m$ has to be chosen such that the integral of $\tilde{\gamma}$ equals the known circulation $\Gamma_b$ or $\Gamma_p$.

## 6. On the influence of viscosity on the span of the endplates

In this section we investigate, be it in an approximate way, the influence of the span of the endplates on the efficiency when viscosity is taken into account. From table 5.4 it follows that the potential theoretical efficiency $\tilde{\eta}(k)$ of the screw propeller in its design situation increases when the span of the endplates $2\Sigma$ with $0 \leq \Sigma \leq 2{,}58$ cm and hence the ratio of covering k, increases. However when the span $2\Sigma$ increases also the viscous resistance of the endplates becomes larger, hence the "physical" efficiency $\eta$ of the propeller will not increase as

fast as is suggested by the increase of $\tilde{\eta}$. In fact it can be expected that for $k = 1 - \delta$, $0 < \delta << 1$, the viscous losses increase faster than the potential theoretical gain. The reason is that in the neighbourhood of the maximum of the potential theoretical efficiency $\tilde{\eta}(k=1)$, this efficiency probably behaves as $\tilde{\eta}(k) = \tilde{\eta}(1) - 0(\delta^2)$. Hence a gain is possible only of $0(\delta^2)$. However the viscous losses increase by $0(\delta)$ for $k \to 1$, which is certainly larger when $\delta$ is sufficiently small. We will investigate the influence of the viscosity on the efficiency somewhat more closely.

We calculate the viscous resistance of the endplates approximately by using a plate resistance formula. We divide the half span (3.75 cm) of the basic planform (figure 4.1) in 5 equal intervals. Then we consider the chordlines through the endpoints of these intervals, which are parallel to (AB). These lines divide the area of the half endplate into five parts with area's $\Delta S_n$ $(n=1,2,\ldots,5)$, where $\Delta S_1$ is next to (AB). These area's are

$$\Delta S_1 = 5.6,\ \Delta S_2 = 5.48,\ \Delta S_3 = 5.23,\ \Delta S_4 = 4.66,\ \Delta S_5 = 3.22 : \text{cm}^2. \tag{6.1}$$

The mean values of the chordlengths of these area's are

$$c_1 = 7.49,\ c_2 = 7.35,\ c_3 = 6.94,\ c_4 = 6.30,\ c_5 = 4.50 : \text{cm}. \tag{6.2}$$

Next we consider the Reynolds numbers $\text{Rey}_n$ $(n=1,\ldots,5)$, these area's with respect to their mean chordlengths $c_n$, namely

$$\text{Rey}_n = \frac{\{U^2 + \omega^2 R^2\}^{1/2}}{\nu} c_n \overset{\text{def}}{=} \frac{Vc_n}{\nu}, \quad (n = 1,\ldots,5), \tag{6.3}$$

where we take for the kinematic viscosity of water $\nu = 1.2\ 10^{-6} \text{m}^2/\text{sec}$. The viscous resistance of one strip of area $\Delta S_n$ can approximately be written as

$$2\,\frac{\rho}{2}\,V^2\,\frac{0.075}{(^{10}\log\,Rey_n-2)^2}\,\Delta S_n \text{ Newton},$$

where the first factor 2 is because the strip has two wetted sides. Now suppose we have a ratio of covering k then we have to multiply (see table 5.1) each strip area $\Delta S_n$ by 0.689 k. It follows from (6.4) that we can write the total viscous resistance F(k) of one endplate as

$$F(k) = 0.689\,k\rho\,V^2\,0.075\sum_{n=1}^{5}\frac{2\Delta S_n}{(^{10}\log\,Rey_n-2)^2} = 2.54\,k \text{ Newton}, \quad (6.5)$$

where now the factor 2 under the summation sign is because each endplate consists of two halves. This resistance acts in the direction (AB) of figure 4.2.

We calculate the extra power $\Delta E_p$ needed for the rotation of the propeller, caused by the viscosity of the water. For that purpose we use the components of the resistance of the endplates perpendicular to the x-axis. We find

$$\Delta E_p = \omega R\pi D\{(\pi D)^2 + (\tfrac{U}{N})^2\}^{-\frac{1}{2}}3F(k) = 86.99\,k \text{ Newton m/sec.} \quad (6.6)$$

There is also the power needed to overcome the viscous resistance of the blades. In our approximation this power is independent of k and therefore it is not important for the following, we denote it by $\Delta E_b$. Then we find the power $E_{tot}$ needed to rotate the propeller

$$E_{tot} = \{\frac{E_a}{q} + \Delta E_p + \Delta E_b\} = \{\frac{221}{q} + 86.99\,k + \Delta E_b\} \text{ Newton m/sec.} \quad (6.7)$$

We now calculate for which value of k the right hand side of (6.7) is minimum, q = q(k) depends also on k (table 5.4).

$$k = 1.00,\ 0.75,\ 050,\ 0.25,\ 0.00,$$
$$(E_{tot} - \Delta E_b) = 351\ ,\ 333\ ,\ 322,\ 323\ ,\ 341\ ,\ \text{Newton m/sec.} \quad (6.8)$$

It follows that a minimum of $E_{tot}$ occurs for a ratio of covering k in between k = 0.5 and k = 0.25.

We mentioned already that endplates become more appropriate for larger values of the thrust. For instance when we take T = 300 Newton, then using (5.6) we find instead of (6.7)

$$E_{tot} = \{\frac{497}{q} + 86.99\ k + \Delta E_b\}\ \text{Newton m / sec.} \qquad (6.9)$$

By this (6.8) changes to (note that q = q(k) is independent of T),

$$k = 1.00,\ 075,\ 0.50,\ 0.25,\ 0.00,$$
$$(E_{tot} - \Delta E_b) = 680\ ,\ 667\ ,\ 671\ ,\ 699\ ,\ 767,\ \text{Newton m/sec.} \qquad (6.10)$$

From (6.10) it is seen that now a minimum of $E_{tot}$ occurs for a larger ratio of covering k, in between k = 0.75 and k = 0.5.

## 7. Camber of profiles of blade and endplate

From section 5 we know the bound vorticity distribution over blades and endplates. This is the component of the vorticity which is perpendicular to the helicoidal lines on the planforms of the blades and on the planforms of the endplates, respectively. Then because the vorticity is free of divergence also the vorticity component along these helicoidal lines is known and also the shed vorticity on the helicoidal lines behind the blades and endplates. This means that all the vorticity is known. The source and sink distributions at the planforms of blades and endplates follow from their thickness distribution.
By this knowledge we are able to formulate a linearized lifting surface theory which yields the camber of the profiles. This has been done by means of the well known vortex and source lattice method.

We still make a remark about the hub. Because we did not put vorticity at the geometrical hub cylinder, the component of the velocity induced by the vorticity and sources, perpendicular to the cylinder will not be zero. From this normal component we can calculate the slope of the flow along a helicoidal line at the hub cylinder. By intergrating this slope we find the shape of the hub for which the camber of blade and endplate profiles as calculated above, will be correct. It is however to be expected that in the working parts of the screw propeller the error will be small when we still take a circular hub for our model used in the experiments.

Some results of the calculation, for the ratio of covering $k = 0.75$, are given in figures 7.1, 7.2, and 7.3. It can be seen that the camberlines of the profiles of the endplate at the low pressure side and at the high pressure side of the blade, are different. This difference of the profiles close to the tip of the blade (figure 7.2, $\sigma/\Sigma = 0.05$ and figure 7.3, $\sigma/\Sigma = -0.05$) will cause a ridge in the middle of the outer side of the endplate. However by keeping the trailing edge of both halves of the endplate at the same level, this ridge is only pronounced in the leading edge region of the midchord of the endplate as can be seen in the photograph of the propeller model (figure 7.4).

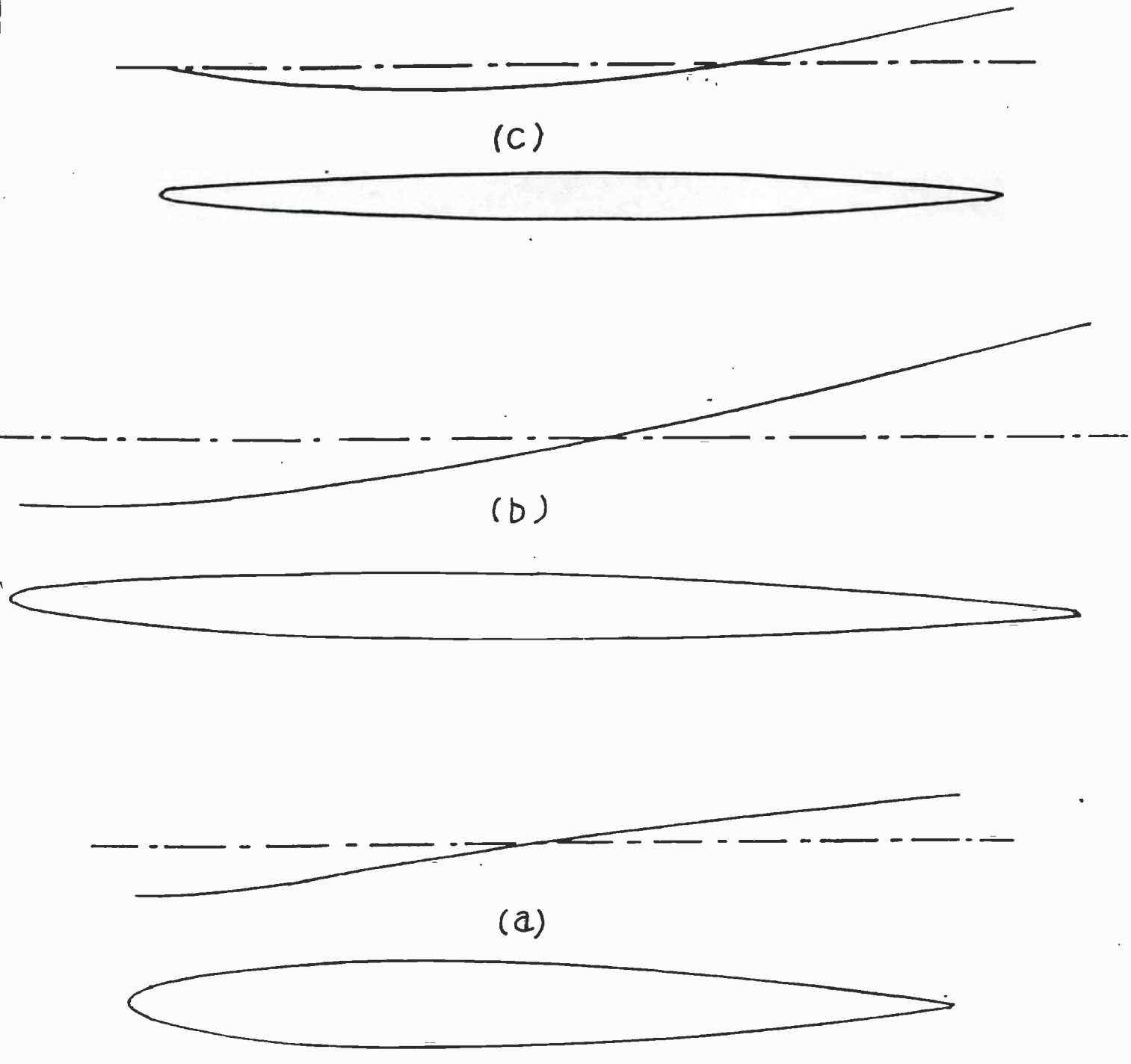


Fig. 7.1. Profiles of screw blade; (a) r/R = 0.225 ;(b) r/R = 0.625;
(c) r/R = 0.99375. Camberlines and thickness distributions.

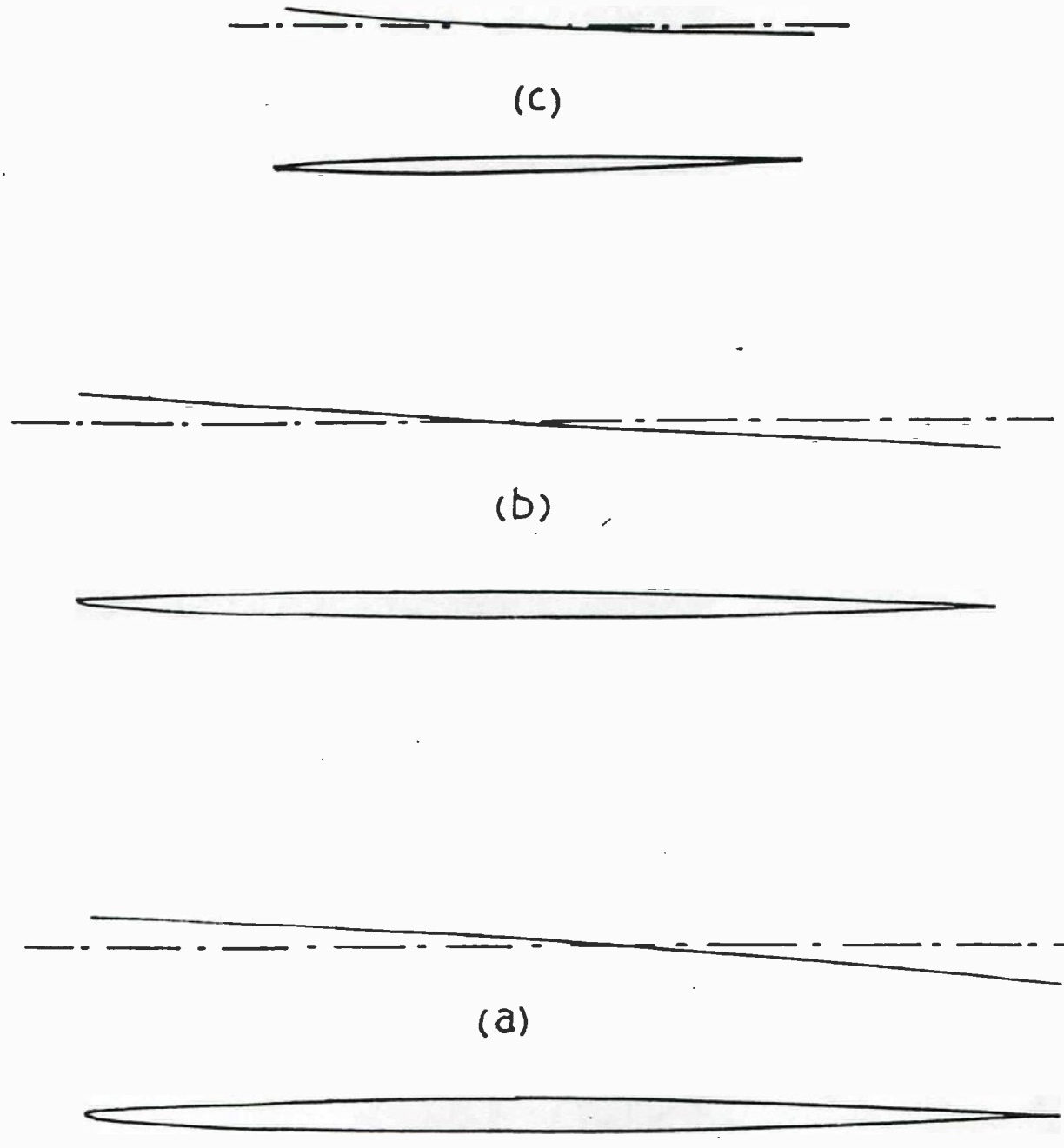


Fig. 7.2. Profiles of end plate, low pressure side of blade; (a) $\sigma/\Sigma = 0.05$; (b) $\sigma/\Sigma = 0.45$; (c) $\sigma/\Sigma = 0.9375$. Camberlines and thickness distributions.

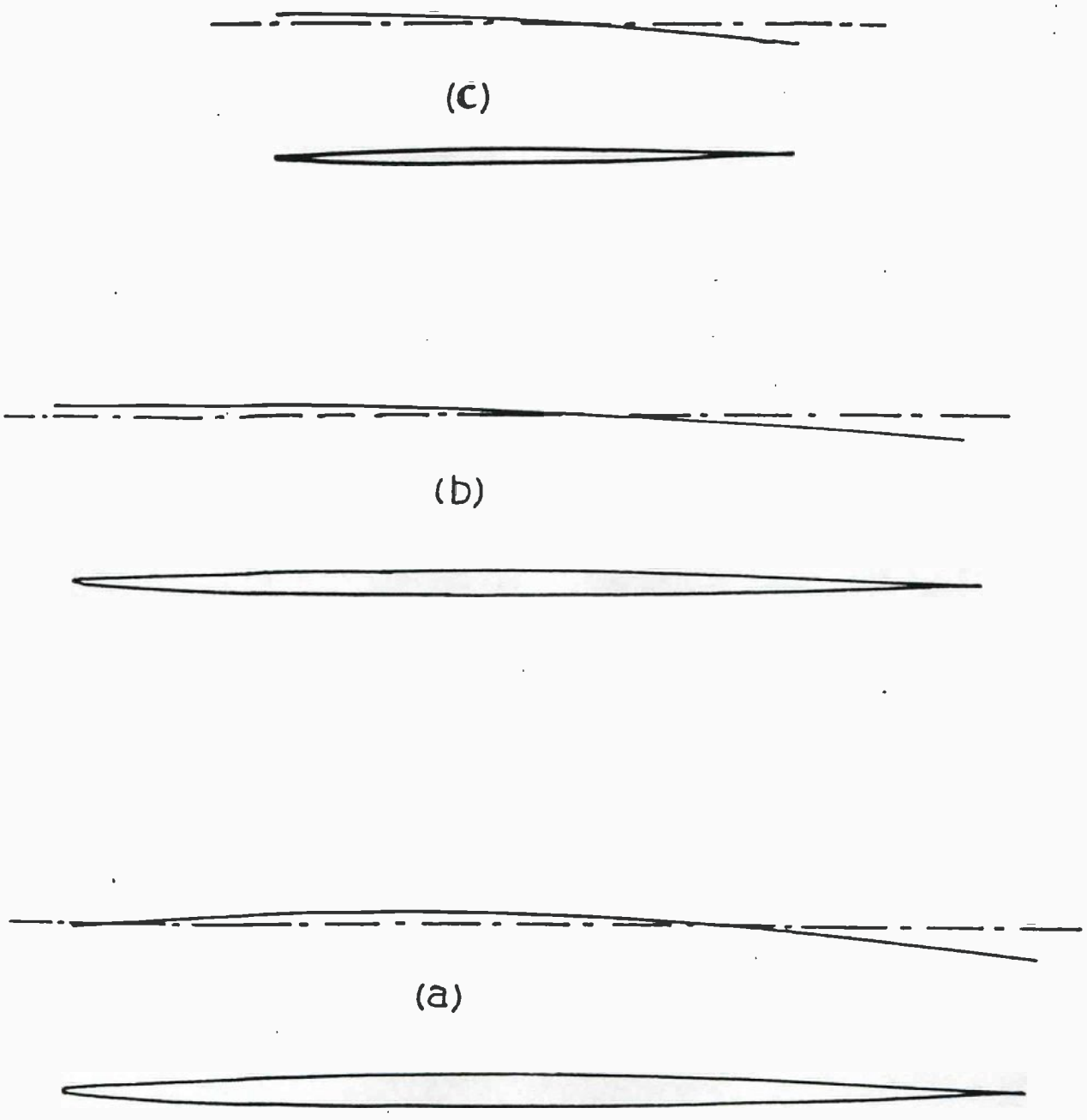


Fig. 7.3. Profiles of endplate, high pressure side of blade; (a) $\sigma/\Sigma = -0.05$; (b) $\sigma/\Sigma = -0.45$; (c) $\sigma/\Sigma = -0.9375$. Camberlines and thickness distributions.

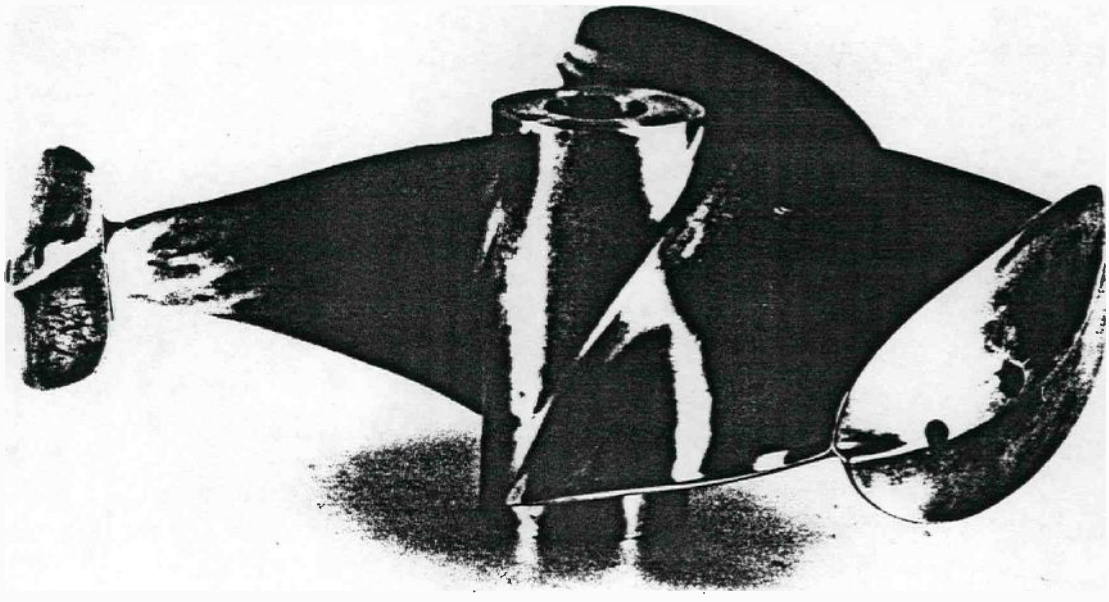

Fig. 7.4. Photo of model screwpropeller.

In figure 4.1 we gave the developed basic planform of the endplate. The endplate we will use in our model propeller is for a ratio of covering k = 0.75. This is larger than the value of k which follows from (6.8). The reason for this is that we first intended to make a number of propellers with decreasing values of the span of the endplates. Due to difficulties in the manufacturing of the propellers we have at our disposal only the propeller with k = 0.75. However it turns out in section 8 that this one is not bad at all. It follows from table 5.1 that the factor by which the transverse dimensions of the developed basic planform of the endplate have to be multiplied is $\mu$ = 0.517. This results in the shape drawn in figure 7.5 where also the calculated tip

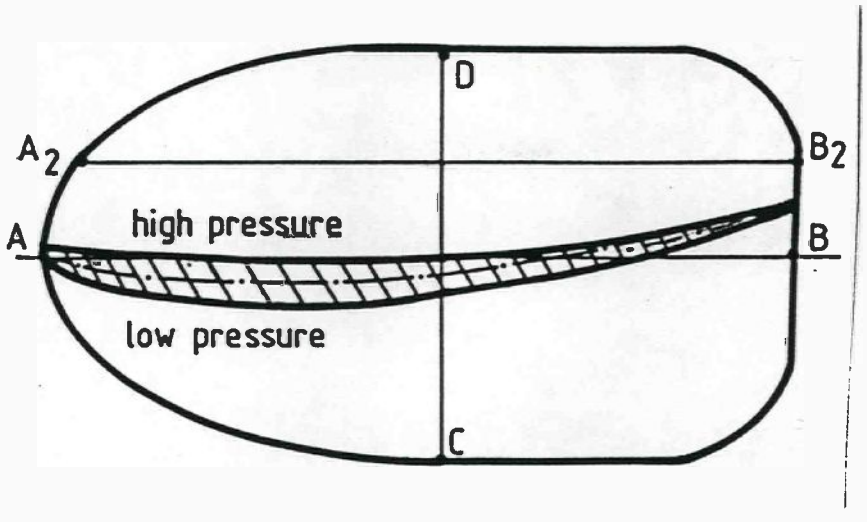


Fig. 7.5. Developed planform of endplate (k = 0.75) with tip profile of blade, |(AB)| = 7.50 cm, |(CD)| = 3.88 cm.

profile of the blade is drawn (figure 7.1 (c)).

We now discuss some difficulties which arise from the assumptions made in the linearized theory with respect to the positions of the profiles of blades and endplates, in other words by satisfying the boundary conditions at the planforms of blades and endplates. In the linearized theory it is assumed that the rather thick and cambered tip profile of the blade coincides with the infinitely thin helicoidal line (AB) in figure 7.5, which forms the tip of the planform of the blade and which is a straight line in the developed planform of the endplate. A profile of the "developed" endplate lies in a plane perpendicular to the plane of drawing of figure 7.5, it coincides in the linear theory for instance with the developed helicoidal line $(A_2B_2)$ which is straight and parallel to (AB). When $(A_2B_2)$ is too close to (AB) it cuts the calculated tip profile of the blade tip and passes from its high pressure side to its low pressure side. Of course this makes no sense.

Another difficulty is that the streamlines just above the endplate and just below it are not nearly parallel but cross each other. The reason is that the disturbances caused by the blade at the inner side of the endplate are rather strong. This means that the concept of a profile of the endplate is lost to some extent.

It follows from the above that our linear results cannot be applied without adaptions to the geometry we used up to now for the endplate. In order to cope with the above mentioned difficulties we have remodelled the endplate by putting its profiles along the mean streamlines above and below the endplate. In the neighbourhood of the blade they follow exactly the blade tip profile.

## 8. Experimental results

First we give some general considerations. We use the following dimensionless quantities

$$J = U/ND,\ K_T = T/\rho N^2 D^4,\ K_Q = Q/\rho N^2 D^5,\ \mathrm{Rey} = \frac{c_r V}{\nu}, \tag{8.1}$$

where Q is the moment exerted at the propeller axis, $c_r$ is the chordlength of the blade at r = 0.85 R = 0.0085 m and $V = \{U^2+\omega^2(0.85)^2\}^{\frac{1}{2}}$ is the velocity of that chord. The value of r/R is taken somewhat larger than is usual for ordinary screw propellers because here the working part of the blade is more in the neighbourhood of the tip. The demanded theoretical design condition corresponds to J = 0.8 and $K_T$ = 0.356. From dimension analysis it follows that for similar screw propellers acting in an unbounded incompressible viscous fluid when cavitation does not occur, we have the relations.

$$\eta = \eta(J,\mathrm{Rey}),\ K_T = K_T(J,\mathrm{Rey}),\ K_Q = K_Q(J,\mathrm{Rey}). \tag{8.2}$$

Consider a propeller which is working in an inviscid fluid and which is optimum with respect to our linear theory. Its diameter is $D_1$, its number of revolutions per second is $N_1$, its velocity is $U_1$ and its delivered thrust is $T_1$. Then we consider another propeller which originates from the previous one by multiplying all dimensions by $\sigma$, where $\sigma$ is some positive number. Hence it is similar to the previous one and its diameter $D_2 = \sigma D_1$. Suppose that the rotational velocity of this latter propeller $N_2 = \tau N_1$, where $\tau$ is some positive number. Then when its velocity $U_2 = \sigma\tau U_1$, it can be shown that the new propeller is again optimum, its thrust $T_2 = \sigma^4\tau^2 T_1$ and its quality number q is the same.

For both propellers of the preceding paragraph J has the same value, hence in an inviscid fluid it follows from (8.2) that $K_T$ is the same, which is in agreement with the two mentioned thrusts $T_1$ and $\sigma^4\tau^2 T_1$. That the second propeller is also optimum is of importance for the application of our results to real propellers.

The model of the screw propeller with endplates, which has a diameter D = 0.2 m has been observed in a cavitation tunnel with a cross section of 0.3 m by 0.3 m. The velocity of the tunnel flow, the number of revolutions per second of the propeller and the ambient pressure in the tunnel, have been adjusted to give a good impression of the shed vorticity in approximately the design condition. The hub vortex which occured was quite normally visible. Tip vortices of the endplates however could be made visible with difficulty by lowering strongly the ambient pressure in the tunnel and only at those half endplates which are at the high pressure sides of the blades. Probably the reason for the difficulty in showing the tip vorticity is that the endplates were designed to have distributed shed vorticity which is important for optimization. Sheet cavitation could be created at the low pressure sides of the blades, but it did not continue on the adjacent parts of the inner sides of the endplates. Also sheet caviation could be realized at the outer sides of those half-endplates which are at the low pressure sides of the blades.

Next we describe some open water tests, hence with the propeller moving in undisturbed water. The axis of the propeller was 24 cm below the water surface, which turned out to be sufficiently deep to avoid free surface effects. There has been carried out two different series of measurements. One for smaller velocities hence for smaller values of Rey, with $N \approx 5.50$/sec and another for larger velocities, hence for larger values of Rey, with $N \approx 18.75$/sec. The results have been drawn in figure 8.1.

From the two series of experiments we consider in each one that experiment of which the value of J is close to the design value J = 0.8. This is for the series with the small velocities, J = 0.801, U = 0.882 m/sec, N = 5.51/sec hence Rey = $0.25\ 10^6$ and for the series with the large velocities J = 0.805, U = 3.025 m/sec, N = 18.79/sec hence Rey = $0.85\ 10^6$. For these two cases we find from the measurements $K_T = 0.294$, $\eta = 0.575$ and $K_T = 0.297$, $\eta = 0.601$, respectively. Hence there is an increase in efficiency of about 2.5% caused by increase in the Reynolds number by a factor 3.4.

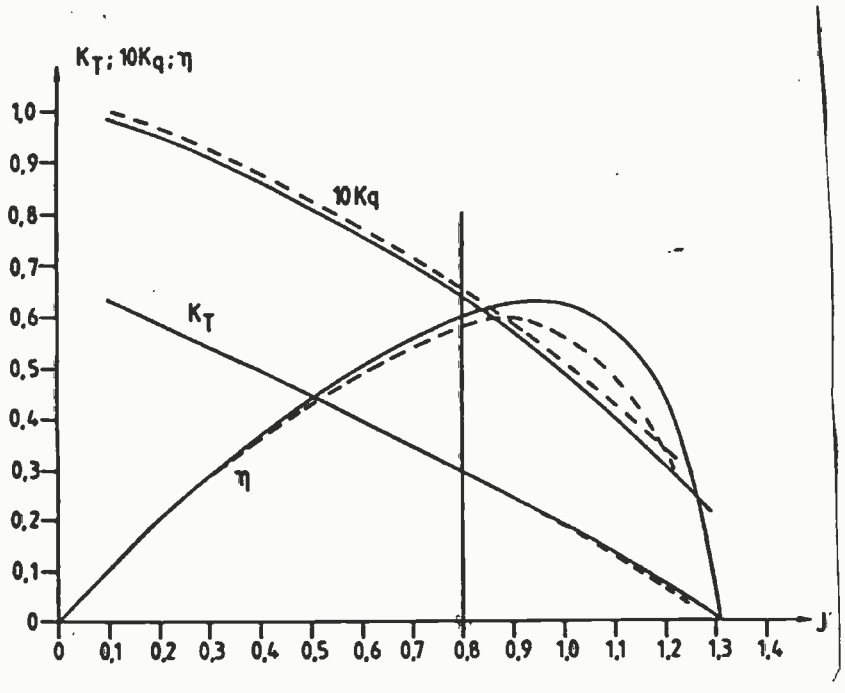


Fig. 8.1. η, $K_T$ and $K_Q$, open water test,
N = 18.75/sec ————————, N = 5.50/sec ------.

It follows from these results that for the design condition with J = 0.8, the value of $K_T \approx 0.30$, which corresponds to a thrust of 168 Newton. It can be calculated easily by the method of section 6 that there is a viscous loss of thrust wich approximately amounts to $\Delta T = 6 + 1.88k = 7.4$ Newton. Hence the delivered potential theoretical thrust of our model screw can be taken as $168 + 7.4 \approx 175$ Newton. This is 25 Newton less than the demanded thrust of 200 Newton. It seems that this deficiency has to be attributed to the shortcomings of the linearized theory, which we hope to correct in the future.

We now accept our model propeller with its thrust of 168 Newton and look for a B-screw series propeller with 3 blades, with the same blade area ratio = 0.65 and which has for J = 0.8 the same value $K_T$ = 0.3 as our model propeller. This is the screw propeller with H/D = 1.372 where H is its pitch. This propeller we call the $B^*$ propeller and our propeller we call the G propeller. The values of $\eta$ and $K_T$ of the $B^*$ and the G propeller are drawn in figure 8.2, where for the G propeller we took the values measured with the larger values of Rey (N = 18.75/sec).

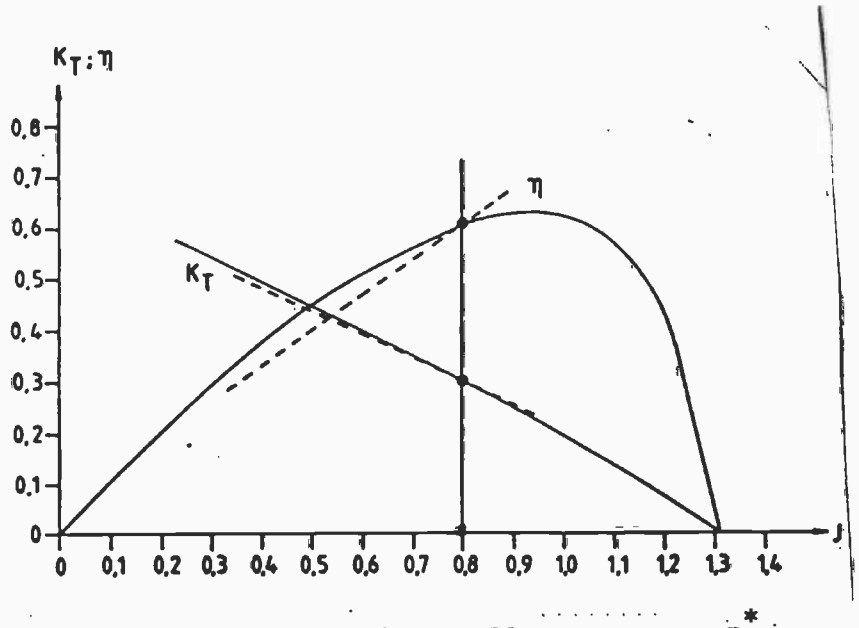


Fig. 8.2. $\eta$,$K_T$ open water test, G propeller ————, $B^*$ propeller -------.

It turns out that for J = 0.8 the efficiency of our G propeller is slightly larger than that of the $B^*$ propeller. The B-screw series however have been tested for Rey $\approx 2\ 10^6$ which is a factor 2.35 larger than the value Rey = $0.85\ 10^6$ for which the G propeller was measured (J=0.8). This means that this difference in efficiency would have been somewhat more in favour of the G propeller (about 1.5%), if the G propeller also had been measured with Rey = $2\ 10^6$. We note that, because the G propeller has its endplates at the tip of its blades, it increases more in efficiency when it is considered at Rey = $2\ 10^6$ than the $B^*$

propeller decreases in efficiency when it is considered at Rey = 0.85 $10^6$. It can be expected that a propeller with endplates will have more advantage of the large Reynolds number when it is used as a real propeller, than a B-screw series propeller.

When we consider both propellers for values of $J < 0.8$ then $K_T$ increases and hence also the thrust. Then it can be expected that the endplates become more effective and that the efficiency of the G propeller will become significantly larger than the efficiency of the $B^*$ propeller. That this is true follows from figure 8.2, where we have to notice that for values of $J < 0.8$ the value of $K_T$ of the G propeller is even larger than the value of $K_T$ of the $B^*$ propeller. Hence for larger loading the propeller with correctly shaped endplates seems indeed to be favourable. Probably this effect would have been smaller when we had taken the ratio of covering k between k = 0.25 and k = 0.5 as follows from (6.8), instead of k = 0.75 as we did.

Finally we give some measurements carried out with the propeller with endplates working behind the model of a tanker with a block coefficient of 0.8. The length of the model was 3 m, its breadth 0.4 m, its immersion at the stern was 20 cm and at the bow 13 cm. This tanker model was positioned in front of the experimental set up which was used for the open water tests. Because the propeller was somewhat too large for the tanker model, it was placed in the plane of the propeller of the tanker but with its axis at the somewhat lower level of 17 cm below the water surface. The number of revolutions per second of the propeller was N = 5.5/sec.

The results of this experiment are given in figure 8.3. Suppose that the ship model moves with the velocity W and that the value of the thrust coefficient is $K_T$. The screw behind the ship encounters the water with "in the mean" a velocity $W_a < W$. This velocity $W_a$ we define by using the experiments of the open water tests in the following way. We put $W_a$ equal to the velocity in the open water test (for N = 5.50/sec), for which the same value $K_T$ occurs as behind the ship model.

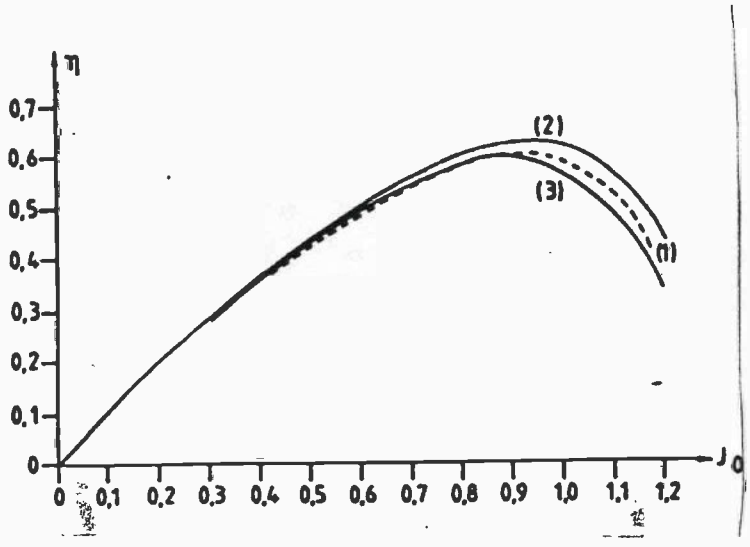


Fig. 8.3. (1) η of screw behind tanker model; (2) η open water test N = 18.75/sec; (3) η open water test, N = 5.50/sec.

An approximation of the effective wake factor $(W-W_a)/W$ for our ship model is

$$(W-W_a)/W = 0,1 + 0.081\ W/ND. \tag{8.3}$$

The efficiency η, curve (1) in figure 8.3, follows from

$$\eta = \frac{TW_a}{Q\omega} = \frac{K_T J_o}{2\pi K_Q}, \tag{8.4}$$

where $K_T$ and $K_Q$ belong to the velocity W of the tanker model and $J_o = W_a/ND$, where $W_a$ corresponds to W in the way as we described above.

Reference

1.L. Klaren and J.A. Sparenberg, On optimum screw propeller with endplates, Journal of Ship Research, Vol. 25, No. 4, Dec. 1981, pp. 252-263.

## Acknowlegdements.

The authors are indebted to the "Shiphydrodynamical Laboratory" of the Technical University of Delft. To Prof. ir. M.C. Meyer for very valuable discussions about the practical aspects of this investigation and for the design of the experiments. To Ing. A. Goeman who carried out the experiments and to Mr. A. Buitenhek and his collaborators, who manufactured the screw blades.

They are also indebted to Ing. A. Klop and his collaborators of the "Central Workshop" of the Technical University of Delft, who manufactured the endplates.

To "Wolfard en Wessels" B.V., for financial support in connection with a grant (project EBSS83-04) of the National Foundation for the Coordination of Maritime Research (C.M.O.).